Ultrafast relaxation kinetics of excited states in a series of mini- and macro-β-carotenes

M. Yoshizawa and H. Aoki

Department of Physics, Graduate School of Science, Tohoku University, Aramaki-aza-aoba, Aoba-ku, Sendai 980-8578, Japan

M. Ue

Department of Materials Science and Chemical Engineering, Faculty of Engineering, Shizuoka University, Johoku, Hamamatsu 432-8561, Japan

H. Hashimoto

"Light and Control," PRESTO/JST, Department of Physics, Graduate School of Science, Osaka City University, 3-3-138 Sugimoto, Sumiyoshi-ku, Osaka 558-8585, Japan

Relaxation kinetics in a series of *all-trans*-carotenes that have excited states with different energies has been investigated using femtosecond absorption and Raman spectroscopy. The dependence on the energies shows that the $1B_u^-$ state plays an intermediate state of the relaxation from the initially photoexcited $1B_u^+$ state to the $2A_g^-$ state. After the relaxation to the $2A_g^-$ state, the excess energy is held in a C=C stretching mode (ν_1) of the $2A_g^-$ state. The lifetime of the ν_1 mode is longer than several picoseconds in short (mini) carotenes, but it is shorter than 1 ps in long (macro) carotenes. Vibrational feature in carotenoids is of importance in energy transfer of photosynthesis, because the excess energy of the photoexcitation is stored in the ν_1 mode during the relaxation kinetics.

I. INTRODUCTION

Carotenoids play an important role in light-harvesting function in bacterial photosynthesis.[1,2] In the antenna complexes of the photosynthesis, light energy is absorbed by *all-trans*-carotenoid and transferred to bacteriochlorophyll with high efficiency.[3–5] It has been generally accepted that the ground state of carotenoids has A_g^- symmetry because of C_{2h} symmetry in analogy to *all-trans*-polyene. The lowest optically allowed singlet excited state is the $1B_u^+$ state, but other two optically forbidden states $1B_u^-$ and $2A_g^-$ exist below the $1B_u^+$ state.[6] Dynamics of the initially photoexcited $1B_u^+$ state has been investigated by time-resolved fluorescence spectroscopy. The lifetime is obtained to be 100–300 fs.[7–9] It is consistent with formation time of the $2A_g^-$ state observed by time-resolved absorption spectroscopy.[10,11] Therefore, the direct internal conversion from the $1B_u^+$ state to the $2A_g^-$ state was proposed in the beginning. However, the theoretical studies have predicted that the $1B_u^-$ state is an intermediate state of the conversion, because the direct conversion to the $2A_g^-$ state is forbidden.[6,12] Recently, the kinetics of the $1B_u^-$ state has been time resolved in β carotene using 10–20 fs tunable pulses.[13]

Initial vibrational relaxation after photoexcitation is of importance in chemical dynamics and energy-transfer processes in molecules, because the photoexcitation generates an excited state with vibrational modes. However, the energy transfer to the bacteriochlorophyll has been considered to occur from the vibrational ground level of the $1B_u^+$ and $2A_g^-$ states assuming the ultrafast vibrational relaxation. Excess vibrational energy has been ignored. The relaxation of the excess energy is roughly classified into two mechanisms. The initial excess energy of the state is localized in a few vibra-

tional modes. The energy redistribution to other vibrational modes takes place first (intramolecular vibrational redistribution) and the state becomes quasithermal equilibrium. Then, the energy dissipation to surrounding medium occurs (vibrational cooling) and the state relaxes to the thermal equilibrium. The vibrational relaxation processes of the excited states in large molecules had been believed to occur within 1 ps for long years, because the relaxations observed by the early femtosecond studies have time constants of shorter than several hundred femtoseconds.[14–16] Recent studies show that the redistribution processes in the lowest singlet excited state (S_1) are not completed within a few picoseconds in some cases.[17–20] Slow vibrational relaxation in the $2A_g^-$ excited state has been observed also in β carotene and neurosporene.[21–23] The vibrational modes of the excited states can have a long lifetime even in large molecules. Systematic investigation of vibrational features is needed to clarify the ultrafast relaxation mechanism in carotenoids. The time-resolved Raman spectroscopy has been recognized as a powerful method for studying vibrational features of photogenerated transient states. However, the ordinary method cannot have enough spectral resolution in a femtosecond region because of transform limit of a single pulse. The time-resolved stimulated Raman spectroscopy can measure Raman signals with femtosecond time resolution and good spectral resolution.[22,24] Moreover, the stimulated Raman signal gives information of populations in vibrational levels. The Raman spectroscopy is very useful to investigate relaxation kinetics of specific vibrational modes.

Linear polyene structure of carotenoids has attracted much interest in relation to conjugated polymers. The dependence on the polyene length has been intensively investigated by steady-state absorption and fluorescence spectroscopy, resonance Raman spectroscopy, and time-resolved

absorption spectroscopy.[6,10,25–27] The energy gaps between the excited states and the ground state decrease with the increasing polyene length. The lifetime of the $2A_g^-$ state becomes shorter in longer carotenoids because of smaller energy gap. However, the relaxation kinetics from the photoexcited $1B_u^+$ state to the $2A_g^-$ state has not been well understood. The energy transfer in the photosynthesis is largely influenced by the energy of the excited states. Therefore, the initial relaxation kinetics in carotenoids and the dependence on the length are important questions.

Here, we present the study of the ultrafast dynamics in a series of carotenes with different polyene lengths. The electronic and vibrational relaxations of the excited states have been investigated using femtosecond absorption and Raman spectroscopy. The roles of the $1B_u^-$ state and the vibrational relaxation in the $2A_g^-$ state are discussed comparing the energies of the $1B_u^+$, $1B_u^-$, and $2A_g^-$ states.

II. EXPERIMENT

Experimental setup of the femtosecond time-resolved absorption and Raman spectroscopy was described in detail elsewhere.[22,24] Briefly, 100-fs seed pulses of a mode-locked Ti:sapphire laser (Avesta) were amplified by a kilohertz regenerative amplifier (Spectra Physics). The amplified pulses were separated into three beams. The second-harmonic pulses (397 nm, 150 fs) of the first beam were used as pump pulses for generating excited states. The second beam passed through an interference filter [794 nm, full width at half maximum (FWHM) 23 cm^{-1}] and was used as the Raman pump pulses. Femtosecond supercontinuum pulses generated from the last beam were used as probe pulses. Raman signal of the excited states was observed as transmittance change induced by the Raman pump pulse. The temporal and spectral resolutions of this method can be improved individually free from transform limit of a single pulse, because they are determined by independent pulses. The temporal response follows the transient population of the excited states with the resolution determined by the durations of pump and probe pulses, while the spectral response depends on the bandwidth of the Raman pump pulse. The temporal and spectral resolutions of the equipment were 250 fs and 25 cm^{-1}, respectively.

The transmittance change due to the stimulated Raman scattering on the Stokes (anti-Stokes) side is generally positive (negative) and called Raman gain (Raman loss). It is caused by the largest population of the vibrational ground level in thermal equilibrium. However, vibrational excited levels cannot be negligible in a femtosecond region. Assuming populations of N_j and N_{j+1} in the j and $j+1$ vibrational levels, respectively, nonlinear susceptibility of the stimulated Raman process between the j and $j+1$ levels is represented as

$$\chi^{(3)}(\omega) \propto \pm \frac{N_j - N_{j+1}}{\omega - (\omega_R \mp \omega_v) + i(\Gamma_v + \Gamma_R)}. \quad (1)$$

Here, ω_v and Γ_v are frequency and bandwidth of the Raman transition, respectively. ω_R and Γ_R are frequency and band-
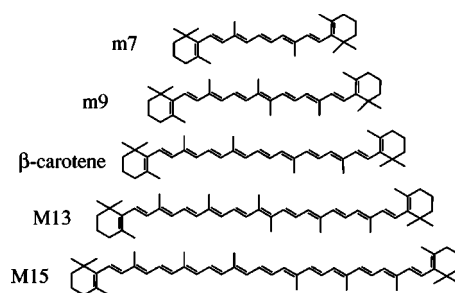

FIG. 1. Chemical structures of *all-trans*-carotenes.

width of the Raman pump pulse, respectively. The signal is assumed to be probed by a δ-function probe pulse. The double signs correspond to the Stokes side (upper) and the anti-Stokes side (lower). The observed transmittance change due to the imaginary part of the nonlinear susceptibility is proportional to the difference of the populations. When the higher level has a larger population ($N_{j+1} > N_j$), the sign of the Raman signal is inverse to that in the thermal equilibrium. It is equivalent to the relation between absorption and stimulated emission in population inversion. Therefore, the transmittance change before the vibrational relaxation should be loss (gain) on the Stokes (anti-Stokes) side.

We have examined shorter and longer homologs of *all-trans*-β-carotene shown in Fig. 1. The homologs are called after the number of the conjugated double bonds n as $m7$ ($n=7$), $m9$ ($n=9$), β carotene ($n=11$), $M13$ ($n=13$), and $M15$ ($n=15$). m and M stand for mini-β-carotene and macro-β-carotene, respectively. β carotene was purchased from Wako Pure Chemical Industries, Ltd., and was recrystallized twice from benzene solution. $m7$, $m9$, $M13$, and $M15$ carotenes were synthesized, respectively, by a reductive dimerization (McMurry reaction) of C15 aldehyde, C18 ketone, C23 ketone, and C25 aldehyde catalyzed by a low-valence titanium compound that was derived from TiCl$_4$.[6] C15 aldehyde and C25 aldehyde were synthesized, respectively, from C13 ketone (β-ionone) and C20 aldehyde (retinal) by the use of Horner-Emmons reaction that was followed by diisobutylaluminum (DIBAL) reduction. β ionone was kindly donated by Kuraray Chemical Co. (Niigata, Japan) and was used after purification by vacuum distillation. Retinal was synthesized by the hydrolysis of retinyl acetate followed by MnO$_2$ oxidation. Retinyl acetate was purchased from BASF Chemical Co. (Switzerland) and was used after purification with silica-gel column chromatography (diethyl ether: n hexane $= 20:80$). C18 ketone and C23 ketone were synthesized, respectively, from C15 aldehyde and C20 aldehyde (retinal) by means of Aldol condensation with acetone.

Benzene solutions of the carotenes were circulated using a 1-mm-flow cell. The measurements were performed at room temperature. The optical density of the solutions in the cell is about 1 at 400 nm. The photon densities of the 397-nm pump pulse and the Raman pump pulse were $2-10 \times 10^{15}$ photons/cm^2 and 6×10^{16} photons/cm^2, respectively. The polarizations of the pump, Raman pump, and probe pulses were parallel to one another. The absorption and fluorescence spectra
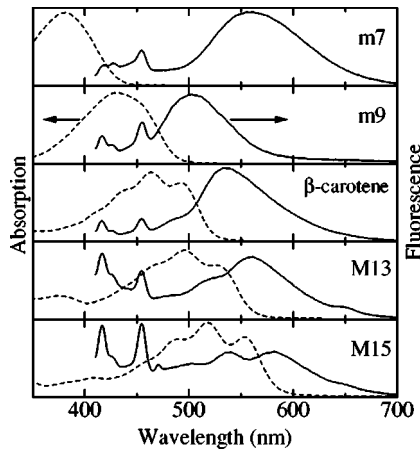
FIG. 2. The steady-state absorption (dashed curves) and fluorescence (solid curves) spectra. Sharp fluorescence peaks around 420–460 nm are due to the spontaneous Raman scattering.

FIG. 3. The time-resolved absorbance changes of $m9$ at the delay times of (a) 0.1–1.0 ps, (b) 1.0–5.0 ps, and (c) 5.0–50 ps.

were recorded with a spectrophotometer (Shimadzu, UVPC2500) and a fluorescence spectrophotometer (JASCO, FP-750), respectively.

III. RESULTS

A. Steady-state absorption and fluorescence spectra

Figure 2 shows steady-state absorption and fluorescence spectra in the carotenes. The absorption spectra in long carotenes ($n \geqslant 11$) have vibronic structures with spacing 1200–1400 cm^{-1}. The lowest-energy peak in each carotene is assigned to the 0-0 vibronic transition from the $1A_g^-$ ground state to the $1B_u^+$ state. The absorption in $m7$ and $m9$ is also assigned to the transition to the $1B_u^+$ state, but the vibronic structure is not clear. The absorption peaks shift to longer wavelength with the increasing length, because the energies of the excited states in the carotenoids are given as a linear function of $1/(2n+1)$, where $2n+1$ is the length of the conjugated polyene.[25]

The fluorescence spectra were measured using a 400-nm excitation light. Sharp peaks around 420–460 nm are due to spontaneous Raman scattering of both the carotenes and the benzene solvent. The fluorescence except $m7$ is assigned to the transition from the $1B_u^+$ state to the ground state. The peaks shift to longer wavelength with the increasing length. However, the fluorescence in $m7$ appears with very large Stokes shift. It is assigned to the transition from the $2A_g^-$ state to the ground state. The $2A_g^-$ state in the exact C$_{2h}$ symmetry is optically forbidden, but the symmetry is expected to be slightly broken in the carotenoids. The fluorescence of the $2A_g^-$ state is observed in short carotenoids because of very long lifetime.[26,27] However, it cannot be observed in long carotenoids because of the small radiative transition rate. In spite of the broken symmetry, we will use the same terminology as for the *all-trans*-polyenes.

B. Femtosecond absorption spectroscopy

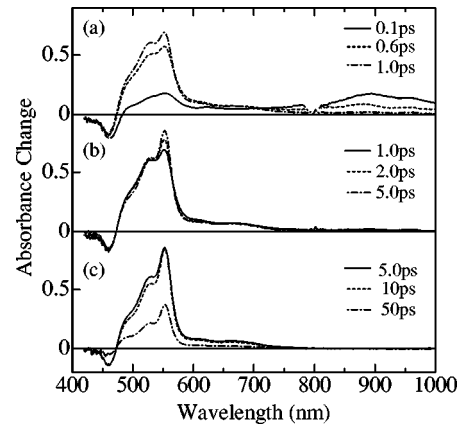The time-resolved absorbance change induced by the 397-nm pump pulse was measured by the same setup with

the time-resolved Raman spectroscopy only blocking the Raman pump pulse by a shutter. Since the pump and probe pulses have parallel polarization, depolarization of the signal may affect the observed kinetics in long delay times. Fluorescence anisotropy of the $2A_g^-$ state in solutions shows that rotation of the carotenoid molecules has time constants of a few hundred picoseconds.[27] Therefore, the polarization effect can be negligible within delay time of a few ten picoseconds.

Figure 3 shows the absorbance changes in $m9$. The relaxation kinetics can be clarified at three stages. In the first stage until the delay time of 1.0 ps (a), a broad absorption band is observed in near-infrared region (800–1000 nm). It appears instantaneously after the photoexcitation and disappears within 1 ps. Another absorption band in visible region (460–600 nm) appears with the decay of the near-infrared band. Bleaching due to the depletion of the $1A_g^-$ ground state appears at 420–460 nm. In the second stage at 1.0–5.0 ps (b), the absorption peak at 550 nm increases and the spectral shape of the visible absorption band becomes sharp. In the last stage (c), the visible absorption and the bleaching decrease with a time constant of several ten picoseconds. The near-infrared and visible absorption bands are assigned to the $1B_u^+$ and/or $1B_u^-$ states and the $2A_g^-$ state, respectively, in the same way as in β carotene.[21,22]

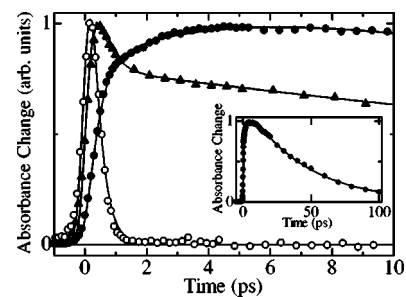Figure 4 shows the temporal absorbance changes in $m9$.

FIG. 4. Transient absorbance changes in $m9$ at 550 nm (closed circles), 610 nm (triangles), and 930 nm (open circles). Solid curves are the best fits to the data assuming exponential rise and decay components. Inset shows the change at 550 nm in the long delay times.

The solid curves are the best fits to the data using exponential rise and decay components with the convolution of the temporal resolution. The resolution at each wavelength was obtained by the crosscorrelation between the pump and probe pulses. It can be represented by a Gaussian function with FWHM of 250–350 fs. The near-infrared absorption at 930 nm appears instantaneously and decreases with a time constant of 0.32 ± 0.05 ps. The peak of the visible absorption band (550 nm) has two rise and one decay components. The fast and slow rises have time constants of 0.3 ± 0.1 ps and 4.3 ± 0.3 ps respectively, and the decay time is obtained to be 44 ps. The fast rise time is consistent with the decay time of the near-infrared absorption. The signal at 610 nm can be fitted to one rise and two decay components. The time constants of the rise and slow decay are consistent with those of the fast rise and the decay at 550 nm, respectively. A time constant of the fast decay is obtained to be 0.4 ± 0.1 ps at 610 nm. However, the fast decay of the visible absorption depends largely on the wavelength. It cannot be represented by a exponential function with a consistent time constant.

The observed kinetics is assigned in the same way in β carotene.[21,22] At the delay times in the first stage, the $1B_u^+$ state is initially photogenerated and the relaxation until the $2A_g^-$ state takes place. Recent studies in β carotene and neurosporene have reported that the first internal conversion from the $1B_u^+$ state to the $1B_u^-$ state occurs within 50 fs followed by the subsequent internal conversion to the $2A_g^-$ state with a few hundred femtoseconds.[12,13] However, they cannot be separated in this study because of the limited temporal resolution. The kinetics in the second stage is assigned to the vibrational relaxation in the $2A_g^-$ state. The $2A_g^-$ state generated by the initial relaxation has large excess energy. The energy is redistributed and dissipated to the solvent. The slow rise at 550 nm is assigned to the dissipation processes in the $2A_g^-$ state. The time constant of the dissipation is estimated to be 4.3 ± 0.3 ps. However, the spectral change due to the redistribution depends largely on the concerned vibrational modes. The redistribution process is difficult to be determined by the observed time-resolved absorbance changes. The decay kinetics in the last stage is assigned to the internal conversion from the $2A_g^-$ state to the $1A_g^-$ ground state. The visible absorption band and the bleaching of the steady-state absorption have the same decay time constant within the experimental errors. However, the observed kinetics may be slightly faster than the population decay of the $2A_g^-$ state because of the depolarization. Considering the error due to the depolarization, the lifetime of the $2A_g^-$ state in $m9$ is estimated to be 44 ± 5 ps

The photoinduced absorbance changes in the series of the carotenes are shown in Fig. 5. They have three common spectral structures (1) the bleaching of the steady-state absorption, (2) the visible absorption band, and (3) the near-infrared absorption band. The photoinduced absorption bands shift to longer wavelength with the increasing polyene length similarly with the steady-state absorption. The visible and near-infrared absorption bands are assigned to the $2A_g^-$ state and the $1B_u^+$ and/or $1B_u^-$ states, respectively.
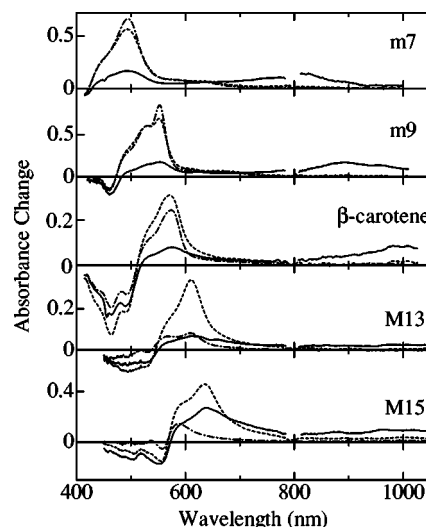

FIG. 5. The time-resolved absorbance changes at the delay times of 0.1 ps (solid curves), 1.0 ps (dashed curves), and 5.0 ps (dashed-dotted curves).

The absorbance changes in the carotenes have similar temporal responses with $m9$ as shown in Fig. 6. The solid curves are the best fits of the data assuming exponential rise and decay components. The time constants obtained by the fits are summarized in Table I. The near-infrared band appears instantaneously and disappears within 1 ps. The visible band appears simultaneously with the decay of the near-infrared signal. It is slightly faster in the carotenes with the middle polyene lengths ($9 \leqslant n \leqslant 13$). The kinetics is assigned to the internal conversion until the $2A_g^-$ state. The lifetime of the $2A_g^-$ state is estimated from the decay of the visible band. It becomes more than 100 times shorter with the in-
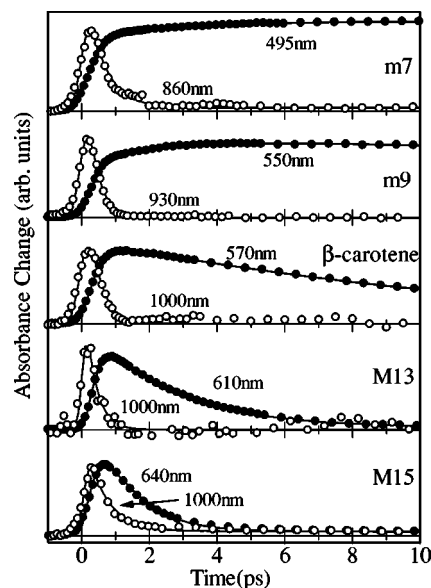

FIG. 6. Transient absorbance changes of the near-infrared signals (open circles) and the visible signals (closed circles). Solid curves are the best fits to the data assuming exponential rise and decay components.

TABLE I. Time constants of relaxation kinetics obtained by the femtosecond absorption spectroscopy.

Sample	Internal conversion (ps)		Vibrational relaxation (ps)
	$1B_u^+$ and/or $1B_u^- \rightarrow 2A_g^-$	$2A_g^- \rightarrow 1A_g^-$	$2A_g^-$
$m7$	0.55 ± 0.05	>230 [a]	6.5 ± 0.5
$m9$	0.32 ± 0.05	44 ± 5	4.3 ± 0.3
β carotene	0.36 ± 0.04	9.0 ± 0.3	~ 1.0
$M13$	0.34 ± 0.05	2.5 ± 0.1	
$M15$	0.53 ± 0.05	0.8 ± 0.1	

[a]The obtained time constant is shorter than the $2A_g^-$ lifetime because of the polarization effect.

creasing polyene length. The spectral change of the visible band is observed in $m7$, $m9$, and β carotene. It is assigned to the vibrational relaxation in the $2A_g^-$ state. The time constants are estimated from the slow rise of the visible absorption peak. However, the spectral change cannot be observed in $M13$ and $M15$ because of the short lifetime of the $2A_g^-$ state.

The absorbance change in $M15$ has a long-lived peak at 590 nm as shown in Fig. 5. The time constant is 36 ± 8 ps. It is much longer than the lifetime of the $2A_g^-$ state. The long-lived absorption has been already observed in other macro-carotenes and assigned to the hot ground state generated after the internal conversion from the $2A_g^-$ state.[10] The long-lived absorption due to the hot ground state is observed also in $M13$ at 560 nm.

The spectral changes observed by the time-resolved absorption spectroscopy is useful to study the energy dissipation. However, it is difficult to investigate the detailed kinetics including the energy redistribution of the specific vibrational modes, because the observed signals are due to transitions from some vibrational levels of the electronic states to another electronic state which is sometimes unknown. Vibrational features of specific vibrational modes in excited states can be investigated by the time-resolved Raman spectroscopy.

C. Femtosecond Raman spectroscopy

The time-resolved Raman signal was measured as the transmittance change induced by the Raman pump pulse. The observed signal consists of sharp lines and broadband. The broadband is assigned to highly excited states generated by the resonant excitation of the Raman pump pulse and is subtracted from the observed signal. The remaining sharp lines are verified to be the stimulated Raman scattering from the temporal and spectral dependence on the Raman pump pulse.[22]

The dash-dotted curves in Fig. 7 show the Raman signals of the ground state in the carotenes. Hatched strong Raman lines at 1590 cm^{-1} are assigned to a nonresonant Raman line of the benzene solvent. The lines around 1500 cm^{-1} in β carotene, $M13$, and $M15$ are assigned to the C=C stretching mode (ν_1) of the ground state. The ν_1 mode in $m7$ and $m9$ is observed as a shoulder of the Raman line of the solvent. Arrows indicate frequencies of the ν_1 mode obtained by stationary spontaneous Raman spectroscopy.

Solid curves in Fig. 7 show transient changes of Raman signals induced by the 397-nm photoexcitation. The changes have two structures. One is negative changes observed in all the carotenes at the arrows. It is assigned to depletion of the ground state. The temporal response of the negative changes shows simultaneous increase with the photoexcitation. Recovery of the depletion in $m7$ and $m9$ has consistent time constants with the recovery of the ground state observed by the time-resolved absorption spectroscopy. However, the recovery times in β carotene, $M13$, and $M15$ are longer than the recovery of the ground-state absorption. It is due to the hot ground state generated after the internal conversion from the $2A_g^-$ state.

Another change is broad signals around 1800 cm^{-1}. They are assigned to the ν_1 mode of the $2A_g^-$ state from the correspondence of the temporal response. $m7$, $m9$, and β carotene have positive and negative peaks around 1800 cm^{-1}. However, the signal in $M13$ has only a positive peak and
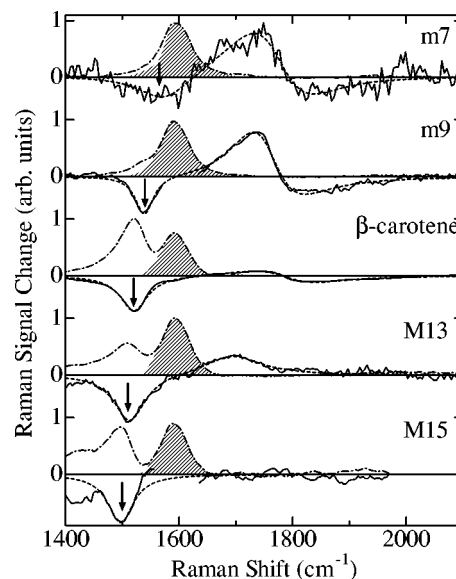

FIG. 7. Photoinduced changes of the stimulated Raman signals. The delay times after the 397-nm photoexcitation are 5 ps in $m7$, $m9$, and β carotene, 3 ps in $M13$, and 1 ps in $M15$ (solid curves). Dashed curves are the best fits to the data assuming the Raman lines with the Lorentzian shape. Dash-dotted curves show the Raman signals of the $1A_g^-$ ground state. Hatched signals are due to the solvent. Arrows indicate the shifts of the ν_1 mode of the ground state obtained by the spontaneous Raman scattering.

TABLE II. Raman shifts and the relaxation times of the ν_1 mode. The vibronic levels of the Raman transitions are indicated in brackets.

Sample	$1A_g^-$ (cm^{-1}) [a]	$2A_g^-$ (cm^{-1}) [b]		Relaxation time (ps)
		Positive	Negative	$1 \rightarrow 0$ of $2A_g^-$
$m7$	1560	1765 ($1 \rightarrow 2$)	1785 ($1 \rightarrow 0$)	~ 10
$m9$	1535	1755 ($1 \rightarrow 2$)	1775 ($1 \rightarrow 0$)	>10
β carotene	1521	1770 ($1 \rightarrow 2$)	1800 ($1 \rightarrow 0$)	>10
$M13$	1512	1695 ($0 \rightarrow 1$)		~ 0.4
$M15$	1503			~ 0.8

[a]Observed by the stationary spontaneous Raman spectroscopy.
[b]Obtained by the best fits to the time-resolved Raman signals. Errors are about 5 cm^{-1}.

$M15$ does not have a clear signal. The Raman signals around 1800 cm^{-1} have been investigated in detail in β carotene.[21,22] At 0.2 ps, the signal has a broad negative peak at 1770 cm^{-1}. Then another negative peak appears at 1800 cm^{-1} and the 1770-cm^{-1} peak becomes positive. The observed signals have been interpreted using two lines at 1770 and 1800 cm^{-1}. The dispersive structure observed at 5 ps is due to the close positive and negative peaks. The positive and negative signals are explained in terms of the vibrational excited levels using Eq. (1). The population in the $j = 1$ vibrational level gives the positive and negative lines due to the $1 \rightarrow 2$ and $1 \rightarrow 0$ Raman transitions, respectively. Therefore, the $2A_g^-$ state in β carotene exists in the $j = 1$ level at 5 ps. Positive and negative Raman signals around 1800 cm^{-1} in $m7$ and $m9$ can be fitted using two lines and assigned to the $1 \rightarrow 2$ and $1 \rightarrow 0$ Raman transitions, respectively, in the same way in β carotene. Lack of the negative signal in $M13$ means that the $2A_g^-$ state relaxes to the $j = 0$ level quickly.

The observed Raman lines are summarized in Table II. The Raman lines in the $1A_g^-$ ground state were measured by the stationary spontaneous Raman scattering. The frequencies in the $2A_g^-$ state were obtained by the fits using Lorentzian functions. Dashed curves in Fig. 7 show the best fits to the spectra. The frequencies in the $2A_g^-$ are about 200 cm^{-1} higher than those in the $1A_g^-$ state. The $1 \rightarrow 2$ and $1 \rightarrow 0$ Raman transitions in the $2A_g^-$ state have anharmonicity. The $1 \rightarrow 2$ transition has 20–30 cm^{-1} smaller frequency than the $1 \rightarrow 0$ transition. The bandwidth in the $2A_g^-$ state obtained by the fits is 120–160 cm^{-1}. It is much broader than that in the ground state.

The time constants of the $1 \rightarrow 0$ vibrational relaxation in the $2A_g^-$ state shown in Table II are roughly estimated from the temporal responses of the Raman signals. The negative changes around 1800 cm^{-1} remain longer than 10 ps in $m7$, $m9$, and β carotene. The ν_1 mode has a very long lifetime in the short carotenes. On the other hand, the positive change in $M13$ appears with the subpicosecond formation time of the $2A_g^-$ state. The unobservable $2A_g^-$ state in $M15$ may be interpreted by nearly equal populations in the $j = 0$ and $j = 1$ levels. The signal due to the depletion of the ground state appears clearly in $M15$, but the signal due to the $2A_g^-$ state is canceled out because of the positive $0 \rightarrow 1$ transition and the

negative $1 \rightarrow 0$ transition. The time constant of the vibrational relaxation in $M15$ is estimated to be about 0.8 ps after the lifetime of the $2A_g^-$ state.

IV. DISCUSSION

The relaxation kinetics observed by the time-resolved absorption spectroscopy has the common processes in all the carotenes, the ultrafast internal conversion from the $1B_u^+$ state and/or $1B_u^-$ state to the $2A_g^-$ state, the vibrational relaxation in the $2A_g^-$ state, and the internal conversion from the $2A_g^-$ state to the $1A_g^-$ ground state. However, the time constants have large difference depending on the polyene length as summarized in Table I. The dependence can be interpreted in terms of the energy levels of the excited states. Figure 8 shows a model of the relaxation kinetics in the carotenes. Solid lines are the schematic energies of the excited states given as a linear function of $1/(2n+1)$, where $2n+1$ is the length of the conjugated polyene.[25] A dashed line represents the $j = 1$ level (ν_1 mode) of the $2A_g^-$ state. The gap between the $2A_g^-$ and $1A_g^-$ states decreases with the increasing length, while the gap between the $1B_u^+$ and $2A_g^-$ states is almost constant. The $1B_u^-$ state changes its energy
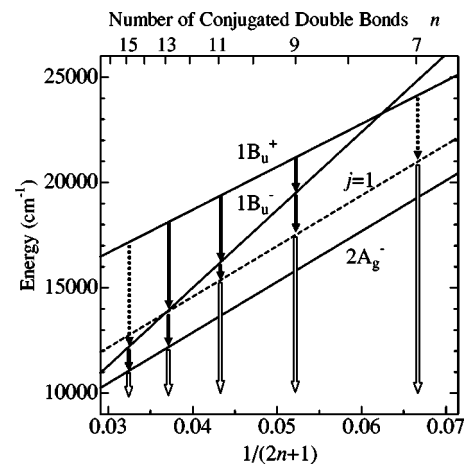

FIG. 8. The dependence on the number of the conjugated double bonds. Solid lines are schematic energies of the excited states and a dashed line represent the vibrational excited level of the $2A_g^-$ state. Arrows indicate the relaxation processes in each carotene.

more largely than the $1B_u^+$ and $2A_g^-$ states and exists above the $1B_u^+$ state in the short carotenes.

The relaxation kinetics after the photoexcitation of the $1B_u^+$ state is represented by arrows in each carotene. The internal conversion from the $2A_g^-$ state to the $1A_g^-$ state (open arrows) has the large dependence on length. The lifetime of the $2A_g^-$ state decreases exponentially with the decreasing energy gap between the $2A_g^-$ and $1A_g^-$ states. The energy of the vibration concerned with the internal conversion is estimated to be about 1600 cm^{-1}. The similar dependence has been already observed in other carotenoids and explained simply by the energy-gap law.[27,28] The vibronic coupling through the ν_1 mode plays a major role in the internal conversion as reported in β carotene.[29]

The internal conversion from the $1B_u^+$ state to the $2A_g^-$ state is represented by the solid and dashed arrows. The time constants are short in the carotenes with the middle length ($9 \leq n \leq 13$). If the direct internal conversion occurs from the $1B_u^+$ state to the $2A_g^-$ state, the almost constant energy gap should give the almost same time constant. Therefore, the $1B_u^-$ state is expected to be a key importance in the relaxation kinetics. In the middle carotenes, the $1B_u^-$ state between the $1B_u^+$ and the $2A_g^-$ states plays as an effective intermediate state. The relaxation to the $2A_g^-$ state takes place as two ultrafast subsequent internal conversions (solid arrows, $1B_u^+ \rightarrow 1B_u^- \rightarrow 2A_g^-$). However, the $1B_u^-$ state in $m7$ cannot be the intermediate state, because it is above the $2A_g^-$ state. The relaxation in $m7$ is relatively slow because of the forbidden internal conversion from the $1B_u^+$ state to the $2A_g^-$ state (dashed arrow). The $1B_u^-$ state in $M15$ can be the intermediate state, but the gap between the $1B_u^+$ and $1B_u^-$ states is larger than the middle carotenes. The relatively slow relaxation in $M15$ (dashed curve) may be due to the large energy gap. Alternatively, the large excess energy of the 397-nm (25 200 cm^{-1}) pump pulse may slow the relaxation in $M15$. When the excess energy remains in the carotenes, alternate internal conversions, $1B_u^+ \rightleftharpoons 1B_u^-$ and $1B_u^- \rightleftharpoons 2A_g^-$, may occur. If so, the relaxation to the lower electronic state is influenced by the redistribution and dissipation of the excess energy. The fluorescence observed above the 0-0 absorption peak in $M15$ suggests that the internal conversion from the $1B_u^+$ state has a similar time constant with the vibrational relaxation. The dependence on the pump photon energy is needed to clarify the initial relaxation.

The time-resolved Raman spectroscopy shows that the ν_1 mode of the $2A_g^-$ state has about 200 cm^{-1} higher frequency than the ν_1 mode of the $1A_g^-$ state. It has been already observed in β carotene and explained in terms of the vibronic coupling between the $2A_g^-$ and $1A_g^-$ states through the A_g symmetric ν_1 mode.[29–31] The coupling pushes down the $j=1$ level of the $1A_g^-$ state and pushes up the $j=1$ level of the $2A_g^-$ state. Therefore, the Raman line of the $2A_g^-$ state has higher frequency. The ν_1 mode of the $2A_g^-$ state has anharmonicity. The $1 \rightarrow 2$ transition has about 20 cm^{-1} smaller frequency than the $1 \rightarrow 0$ transition. It can be interpreted by smaller vibronic coupling in higher vibrational lev-

els. The $1 \rightarrow 2$ Raman transition of the $2A_g^-$ state has lower frequency than the $1 \rightarrow 0$ Raman transition, because of smaller shift. The broad bandwidth in the $2A_g^-$ state suggests ultrafast dephasing or mixture of several lines. However, it has not been well understood.

The vibrational relaxation is generally classified into the energy redistribution to other vibrational modes and the energy dissipation to solvent. The observed spectral changes of the visible absorption band have subpicosecond and several picoseconds time constants. The fast and slow processes may be assigned to the redistribution and to the energy dissipation, respectively. However, the time-resolved Raman signals show that the ν_1 mode of the $2A_g^-$ state remains in the excited level longer than 10 ps in $m7$, $m9$, and β carotene. Therefore, the spectral changes of the visible absorption are assigned to the vibrational relaxation of other than the ν_1 mode. The long-lived ν_1 mode means the small interaction with other modes. The ν_1 mode in the carotenes is a totally symmetric C=C stretching mode (A_g) and localized at the center.[29] The slow vibrational redistribution has been observed in similar vibrational modes in other molecules. The C=C stretching mode in *trans*-stilbene and bacteriorhodopsin has the relaxation time longer than several picoseconds.[20,32] The excess energy in deoxyhemoglobin is localized in the A_{1g} normal modes (ν_4, ν_7).[19] The symmetry and localization may be keys of the small interaction. On the other hand, the ν_1 mode in $M13$ and $M15$ has the short lifetime. It can be interpreted in terms of the $1B_u^-$ state. The $1B_u^-$ state in $M13$ and $M15$ lies below the $j=1$ level of the $2A_g^-$ state. Therefore, the internal conversion between the $1B_u^-$ and $2A_g^-$ states can relax the carotenes until the $j=0$ level of the $2A_g^-$ state.

The relaxation kinetics in the carotenes can be summarized as follows. The initially photoexcited $1B_u^+$ state relaxes to the $2A_g^-$ state passing through the $1B_u^-$ state. However, the direct internal conversion occurs in the short carotenes ($n \leq 7$), because the $1B_u^-$ state is above the $1B_u^+$ state. The excess energy after the internal conversion is held in the ν_1 vibrational mode during the relaxation kinetics, because the energy redistribution from the ν_1 mode exists very slow in the carotenes. However, the long carotenes ($n \geq 13$) has the fast vibrational relaxation because of the low-lying $1B_u^-$ state. Then, the internal conversion from the $2A_g^-$ state to the $1A_g^-$ ground state occurs. It is very fast in the long carotenes because of the small energy gap. Finally, the vibrational relaxation of the ground state occurs with the time constant of several ten picoseconds.

V. CONCLUSIONS

The ultrafast relaxation kinetics in a series of carotenes has been investigated by the femtosecond study. The relaxation from the photoexcited $1B_u^+$ state to the $2A_g^-$ state is faster in the carotenes with the middle polyene lengths ($m9$, β carotene, and $M13$). The negative stimulated Raman signals due to the vibrational excited level of the $2A_g^-$ state have been observed in the short carotenes ($m7$, $m9$, and β

carotene). The relaxation from the $2A_g^-$ state to the ground state becomes fast with the increasing polyene length because of the energy-gap law. The relaxation kinetics in the carotenes is interpreted considering the energy level of the $1B_u^-$ state. The $1B_u^-$ state plays very important roles in the initial relaxation kinetics. It is the intermediate state in the relaxation from the photoexcited $1B_u^+$ state to the $2A_g^-$ state and assists the vibrational relaxation of the $2A_g^-$ state. Without the assistance of the $1B_u^-$ state, the ν_1 mode of the $2A_g^-$ state has very long lifetime in the carotenes. The vibration of the excited states affects largely the interaction with other molecules, because it changes the energy and symmetry. The vibrational excited levels should be considered in the energy transfer in the photosynthesis. The vibration of the electronic excited states relaxes very fast generally, but the specific mode can have long lifetime even in large molecules. The individual measurement of the specific mode using the time-resolved vibrational spectroscopy is necessary to investigate the ultrafast dynamics of the excited state.

[1] Y. Koyama, M. Kuki, P.O. Andersson, and T. Gillbro, Photochem. Photobiol. **63**, 243 (1996).

[2] H.A. Frank and R.J. Cogdell, Photochem. Photobiol. **63**, 257 (1996).

[3] M. Ricci, S.E. Bradforth, R. Jimenez, and G.R. Fleming, Chem. Phys. Lett. **259**, 381 (1996).

[4] J.-P. Zhang, R. Fujii, P. Qian, T. Inaba, T. Mizoguchi, Y. Koyama, K. Onaka, Y. Watanaba, and H. Nagae, J. Phys. Chem. B **104**, 3683 (2000).

[5] H.H. Bilsten, D. Zigmantas, V. Sundström, and T. Polívka, Chem. Phys. Lett. **355**, 465 (2002).

[6] T. Sashima, Y. Koyama, T. Yamada, and H. Hashimoto, J. Phys. Chem. B **104**, 5011 (2000).

[7] H. Kandori, H. Sasabe, and M. Mimuro, J. Am. Chem. Soc. **116**, 2671 (1994).

[8] S. Akimoto, I. Yamazaki, S. Takaichi, and M. Mimuro, Chem. Phys. Lett. **313**, 63 (1999).

[9] S. Akimoto, I. Yamazaki, T. Sakawa, and M. Mimuro, J. Phys. Chem. A **106**, 2237 (2002).

[10] P.O. Andersson and T. Gillbro, J. Chem. Phys. **103**, 2509 (1995).

[11] J.-P. Zhang, C.-H. Chen, Y. Koyama, and H. Nagae, J. Phys. Chem. B **102**, 1632 (1998).

[12] J.-P. Zhang, T. Inaba, Y. Watanabe, and Y. Koyama, Chem. Phys. Lett. **332**, 351 (2000).

[13] G. Cerullo, D. Polli, G. Lanzani, S. De Silvestri, H. Hashimoto, and R.J. Cogdell, Science (Washington, DC, U.S.) **298**, 2395 (2002).

[14] T. Elsaesser and W. Kaiser, Annu. Rev. Phys. Chem. **42**, 83 (1991).

[15] A.M. Weiner and E.P. Ippen, Chem. Phys. Lett. **114**, 456 (1985).

[16] C.H. Brito-Cruz, R.L. Fork, W.H. Knox, and C.V. Shank, Chem. Phys. Lett. **132**, 341 (1986).

[17] T. Nakabayashi, H. Okamoto, and M. Tasumi, J. Phys. Chem. A **101**, 3494 (1997).

[18] H. Hayashi, T.L. Brack, T. Nogichi, M. Tasumi, and G.H. Atkinson, J. Phys. Chem. **95**, 6797 (1991).

[19] M.C. Schneebeck, L.E. Vigil, and M.R. Ondrias, Chem. Phys. Lett. **215**, 251 (1993).

[20] J. Qian, S.L. Schultz, and J.M. Jean, Chem. Phys. Lett. **233**, 9 (1995).

[21] M. Yoshizawa, H. Aoki, and H. Hashimoto, Phys. Rev. B **63**, 180301 (2001).

[22] M. Yoshizawa, H. Aoki, and H. Hashimoto, Bull. Chem. Soc. Jpn. **75**, 949 (2002).

[23] F.S. Rondonuwu, Y. Watanabe, J.-P. Zhang, K. Furuichi, and Y. Koyama, Chem. Phys. Lett. **357**, 376 (2002).

[24] M. Yoshizawa and M. Kurosawa, Phys. Rev. A **61**, 013808 (2000).

[25] P. Tavan and K. Schulten, J. Chem. Phys. **85**, 6602 (1986).

[26] P.O. Andersson, T. Gillbro, A.E. Asato, and R.S.H. Liu, J. Lumin. **51**, 11 (1992).

[27] P.O. Andersson, S.M. Bachilo, R.-L. Chen, and T. Gillbro, J. Phys. Chem. **99**, 16 199 (1995).

[28] V. Chynwat and H.A. Frank, Chem. Phys. **194**, 237 (1995).

[29] H. Nagae, M. Kuki, J.-P. Zhang, T. Sashima, Y. Kumai, and Y. Koyama, J. Phys. Chem. A **104**, 4155 (2000).

[30] H. Hashimoto and Y. Koyama, Chem. Phys. Lett. **163**, 251 (1989).

[31] T. Noguchi, S. Kolaczkowski, C. Arbour, S. Aramaki, G.H. Atkinson, H. Hayashi, and M. Tasumi, Photochem. Photobiol. **50**, 603 (1989).

[32] T. Kobayashi, T. Saito, and H. Ohtani, Nature (London) **414**, 531 (2001).